Detection of metastable electronic states by Penning trap mass spectrometry

https://doi.org/10.1038/s41586-020-2221-0

Received: 15 January 2020

Accepted: 11 March 2020

Published online: 6 May 2020

Check for updates

R. X. Schüssler[1]✉, H. Bekker[1,7], M. Braß[2], H. Cakir[1], J. R. Crespo López-Urrutia[1], M. Door[1], P. Filianin[1], Z. Harman[1], M. W. Haverkort[2], W. J. Huang[1], P. Indelicato[3], C. H. Keitel[1], C. M. König[1], K. Kromer[1], M. Müller[1], Y. N. Novikov[4,5], A. Rischka[1,8], C. Schweiger[1], S. Sturm[1], S. Ulmer[6], S. Eliseev[1]✉ & K. Blaum[1]

State-of-the-art optical clocks[1] achieve precisions of 10^{-18} or better using ensembles of atoms in optical lattices[2,3] or individual ions in radio-frequency traps[4,5]. Promising candidates for use in atomic clocks are highly charged ions[6] (HCIs) and nuclear transitions[7], which are largely insensitive to external perturbations and reach wavelengths beyond the optical range[8] that are accessible to frequency combs[9]. However, insufficiently accurate atomic structure calculations hinder the identification of suitable transitions in HCIs. Here we report the observation of a long-lived metastable electronic state in an HCI by measuring the mass difference between the ground and excited states in rhenium, providing a non-destructive, direct determination of an electronic excitation energy. The result is in agreement with advanced calculations. We use the high-precision Penning trap mass spectrometer PENTATRAP to measure the cyclotron frequency ratio of the ground state to the metastable state of the ion with a precision of 10^{-11}—an improvement by a factor of ten compared with previous measurements[10,11]. With a lifetime of about 130 days, the potential soft-X-ray frequency reference at 4.96×10^{16} hertz (corresponding to a transition energy of 202 electronvolts) has a linewidth of only 5×10^{-8} hertz and one of the highest electronic quality factors (10^{24}) measured experimentally so far. The low uncertainty of our method will enable searches for further soft-X-ray clock transitions[8,12] in HCIs, which are required for precision studies of fundamental physics[6].

Modern clocks and frequency standards range from ensembles of neutral particles trapped in optical lattice clocks[5,13] to individual, singly charged ions confined in Paul traps[14]. With a fractional frequency accuracy of 10^{-18}, such clocks enable stringent tests of fundamental symmetries (for example, Lorentz invariance[15]), geodetic measurements[16] and searches for new physics[17] and dark matter[18]. The transitions used as frequency references typically have long lifetimes, of the order of seconds, yielding sub-hertz linewidths; a recent example is the Yb^+ clock[15,19]. Optical clocks use variations of the Ramsey method, driving such forbidden transitions through stimulated absorption and emission much faster than the natural transition rate, but maintaining the very long coherence times needed for the interrogation schemes owing to their small spontaneous emission rates[1]. One promising species for use in the next generation of clocks is HCIs[6] because their compact size in comparison with atoms makes them less sensitive to external field fluctuations. Several transitions have been proposed to feature a high sensitivity to a variation of fundamental constants[20,21].

Although electronic binding energies in HCIs typically amount to several kiloelectronvolts[22] and inter-shell transitions usually appear in the X-ray region, there are also intra-shell fine and hyperfine transitions in the optical and ultraviolet range[23–27]. Furthermore, some HCIs feature level crossings[6,28] with associated optical transitions. Most of these transitions are electric dipole (E1)-forbidden, and many are of the magnetic dipole (M1) type, with lifetimes of the order of milliseconds, but some are highly forbidden and can have extremely long lifetimes of up to millions of years[17], as predicted theoretically. A few of these transitions with lifetimes ranging from milliseconds to seconds have been found and investigated using storage rings[29] and ion traps[30,31], but so far no method has enabled a direct observation of the excitation energy of extremely long-lived metastable states.

It is difficult to theoretically predict such electronic energies in HCIs. Calculations suffer from difficulties related to strong relativistic contributions and complex correlations of several active electrons in open shells. Moreover, experimental identification of such transitions is challenging because their long lifetimes leads to sub-hertz linewidths and therefore requires very precise application of the Ritz–Rydberg method[32] to other, accurately known transitions to establish the searching range to be explored with narrow-linewidth spectroscopy lasers. Additionally, rough calculations with the flexible atomic code[33] can be used to estimate the energy of transitions.

Here we demonstrate how high-precision Penning trap mass spectrometry directly identifies a suitable clock transition in HCIs by

[1]Max Planck Institute for Nuclear Physics, Heidelberg, Germany. [2]Institute for Theoretical Physics, Heidelberg University, Heidelberg, Germany. [3]Laboratoire Kastler Brossel, Sorbonne Université, CNRS, ENS-PSL Research University, Collège de France, Paris, France. [4]Petersburg Nuclear Physics Institute, Gatchina, Russia. [5]St Petersburg State University, St Petersburg, Russia. [6]RIKEN, Fundamental Symmetries Laboratory, Wako, Japan. [7]Present address: Department of Physics, Columbia University, New York, NY, USA. [8]Present address: ARC Centre for Engineered Quantum Systems, School of Physics, The University of Sydney, Sydney, New South Wales, Australia. ✉e-mail: rima.schuessler@mpi-hd.mpg.de; sergey.eliseev@mpi-hd.mpg.de

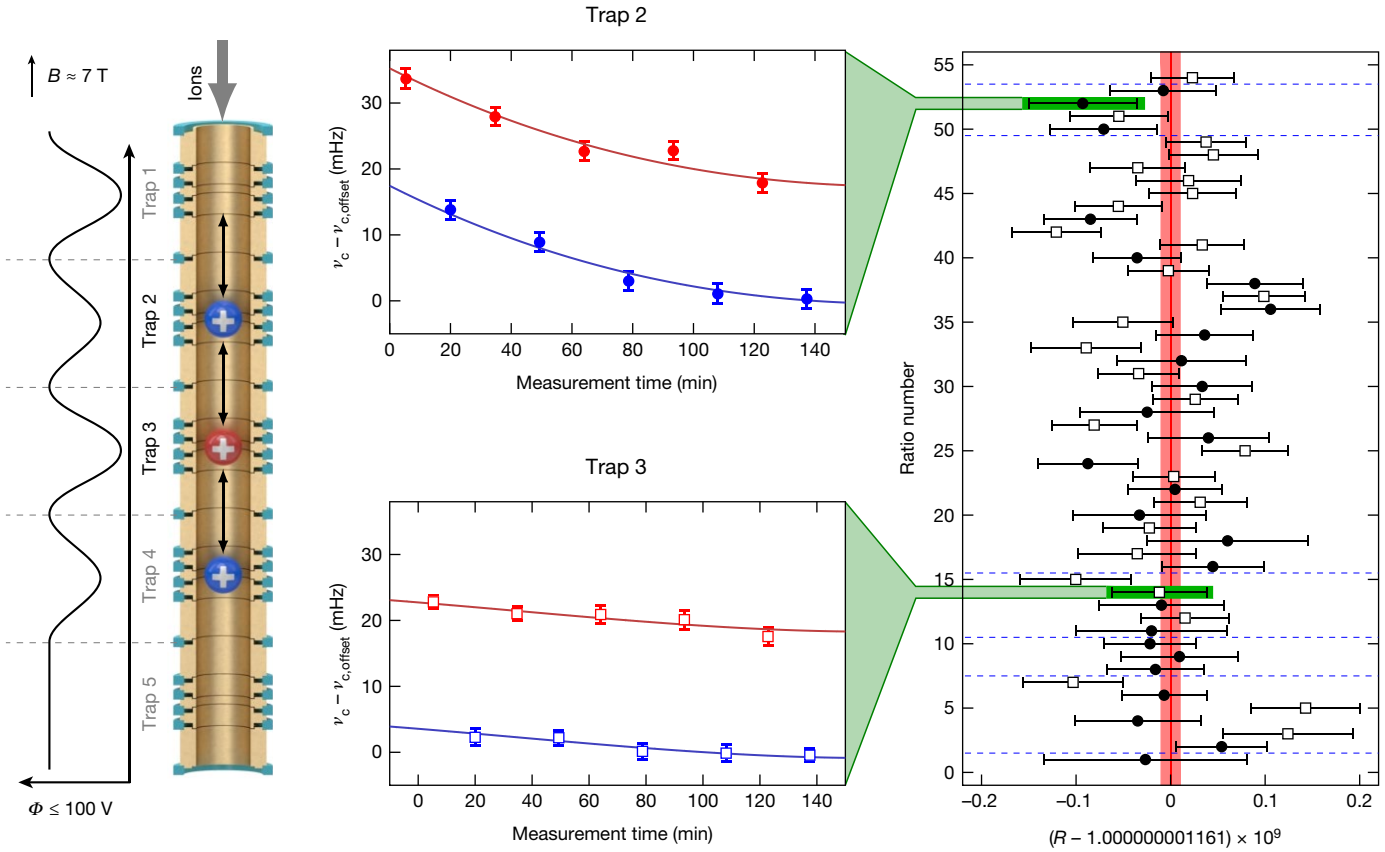

Fig. 1 | Results of the Re measurements at PENTATRAP. All error bars indicate 1σ uncertainty; for details see text. Left, three $^{187}Re^{29+}$ ions (ion 1, blue; ion 2, red; ion 3, blue) are loaded from the top into the trap stack. For each measurement trap, the potential Φ of the neighbouring traps is nominally identical; that is, the potential of trap 2 is also applied in trap 4. The magnetic field points along the direction of the trap axis. Centre, by shifting the ions one trap down or up after a cyclotron frequency determination, we obtain measurements with ion 1 (blue) and ion 2 (red) in trap 2 and with ion 2 (red) and ion 3 (second blue ion) in trap 3. Here, the ion 2 is in the ground state (red) and the other two (blue) are in the metastable electronic state. Right, all ratios (n = 54) determined over seven measurement campaigns (divided by the dashed lines) display the stability of the system. The results for trap 2 (filled symbols) and trap 3 (empty symbols) show a similar behaviour. The final weighted mean is shown in red.

determining the mass difference of a $^{187}Re^{29+}$ ion in the ground state and a metastable state to a precision below 2 eV or ~500 THz. A relative mass measurement of the two HCI states with an unprecedented precision of 1×10^{-11} is achieved by determining the cyclotron frequency $\nu_c = qB/(2\pi m)$ of the HCI with mass m and charge q in a strong magnetic field ($B \approx 7$ T) and a weak electrostatic harmonic potential of the Penning trap. The cyclotron frequency is derived by measuring the ion trap frequencies (modified cyclotron frequency, $\nu_+ \approx 16$ MHz; axial frequency, $\nu_z \approx 700$ kHz; magnetron frequency, $\nu_- \approx 10$ kHz) and applying the invariance theorem[34] $\nu_c^2 = \nu_+^2 + \nu_z^2 + \nu_-^2$.

Penning trap mass spectrometer PENTATRAP

This work was carried out using the high-precision Penning trap mass spectrometer PENTATRAP at the Max-Planck-Institut für Kernphysik in Heidelberg. HCIs produced in the commercial electron beam ion trap DreEBIT[35] using the MIVOC technique[36] are extracted in 1-µs-long bunches with a kinetic energy of a few kiloelectronvolts per charge, selected according to their charge-to-mass ratio, q/m, by means of a 90° dipole magnet, and sent into the Penning traps. Prior to the trapping of the ions, their kinetic energy is reduced to a few electronvolts per charge by appropriately timed pulsed potentials applied to two cylindrical drift tubes. The 4-K cold bore of the superconducting magnet houses five cylindrical Penning traps[37,38]. Two of them (traps 2 and 3; see Fig. 1) are used to measure the trap frequencies of the ions of interest. Traps 1 and 4 serve to store ions, whereas trap 5 will allow monitoring fluctuations of the trap potentials and the magnetic field in the future. To reduce temporal variations of the magnetic field in the traps, the temperature in the laboratory is kept constant at a level of 0.1 K per day. Furthermore, the level of liquid helium and the helium pressure inside the magnet cold bore are stabilized at a level of a fraction of a millimetre and 20 µbar, respectively. These measures reduce fractional changes of the magnetic field in the measurement traps to values of less than a few parts in 10^{10} per hour, resulting in a cyclotron frequency drift of only a few millihertz per hour at $\nu_c = 16$ MHz. Because the magnet is actively shielded with a shielding factor of 50, the fractional fluctuation of the magnetic field in the trap due to the fluctuation of the stray magnetic field does not exceed 3 parts in 10^{11}.

The measurement procedure of the cyclotron frequency ratio of two different ion states consists of the preparatory and the main phase. During the preparatory phase, three ions in the two states are first loaded into the three innermost traps (ion 1 in trap 2 and ion 3 in trap 4 being in the same state—for example, the ground state—whereas ion 2 in trap 3 being in the other state). The desired ion states are confirmed by a rough determination of their respective cyclotron frequencies; if they are not in the desired state, ions are reloaded. After that, their trap motion amplitudes are reduced (the ions are 'cooled') by coupling the magnetron and cyclotron motions to the axial motion, which in turn is brought into thermal equilibrium with a tank circuit having a temperature of around 6 K. The resonance frequency of the tank circuit is approximately equal to that of the axial motion. The axial, magnetron and cyclotron amplitudes of cooled $^{187}Re^{29+}$ ions are approximately

10 μm, 2 μm and 2 μm, respectively. Great care is taken to prepare only a single ion of interest in each trap, because the presence of another undesired ion in the trap would disturb the motion of the ion of interest and hence alter its motional frequencies. The main phase is devoted to the measurement of the ion trap frequencies in traps 2 and 3. The reduced cyclotron and axial frequencies are simultaneously measured by means of the pulse-and-phase[39] and dip[40] techniques, respectively. This minimizes systematic shifts arising from changes in the external fields compared with sequential measurements of the trap frequencies. The measurement cycle consists of a set of sub-measurements. First, the cyclotron motion is excited to an amplitude of approximately 10 μm with a subsequent measurement of its phase (reference phase). It is followed by the re-cooling of all three motions. After that, the cyclotron motion is again excited to the same amplitude and is allowed to freely evolve its phase for 40 s during the subsequent measurement (measurement phase). During the phase evolution time of 40 s, the axial frequency is measured with the dip method. The measurement cycle is ended by re-cooling all ion motions. Because the relative mass difference between the ground and metastable states is at the level of 10^{-9}, it is sufficient to measure the smallest trap frequency—the magnetron frequency—once a day with a moderate precision for the determination of the cyclotron frequency ratio. Ten measurement cycles constitute a measurement run. A unique feature of PENTATRAP is that during each run, frequency measurements are performed simultaneously in synchronized traps—for instance, on ion 1 in trap 2 (upper blue ion in Fig. 1) and ion 2 (red) in trap 3—for approximately 12 min. After that, the ion species are swapped between traps 2 and 3 by moving the three ions adiabatically one trap up. Then, a measurement run is carried out with ion 2 in trap 2 and ion 3 (lower blue ion) in trap 3. Lastly, the ion species are swapped back by moving the three ions one trap down again. After each change of the configuration of ions in the traps, the ion motions are cooled for 20 s. In this way, one alternately determines the cyclotron frequencies of ions in the ground and metastable states in each measurement trap. This measurement sequence is repeated until the measurement is stopped, given that—even though the vacuum allows storage times of several hours to days—ions are then lost owing to charge-exchange reactions with background gas. If determination of the metastable state is no longer possible, the traps are emptied and a new set of ions is loaded.

Energy of the metastable state

To obtain the cyclotron frequency ratio of the ions in the ground and metastable states, the polynomial method described, for instance, in refs. [10,11,41] is applied in the following way. We treat the two measurement traps independently. The temporal variation of the magnetic field—and hence the cyclotron frequency—is approximated with a low-order polynomial, as shown in the middle plots of Fig. 1. This assumption is based on our experience with the magnetic field evolution over a scale of a few hours. The full set of measured cyclotron frequencies is divided into groups. The group length must be as short as possible, such that it can be described by a low-order polynomial, but must contain substantially more data points than the polynomial degrees of freedom. Thus, each group is chosen to be approximately 2 h long and to contain ten cyclotron frequency points (five points correspond to the ion in the ground state and five to the ion in the metastable state); see middle plots of Fig. 1. We use third-grade polynomials because this is the lowest order that has at least one inflection point. Data points from ions in both the metastable and the ground state are fitted with the same polynomial using global fitting parameters. The polynomial for the data points from the ion in the ground state is scaled with an additional fitting parameter R, which corresponds to the frequency ratio. This yields three quantities: (1) the frequency ratio R, (2) its uncertainty ΔR and (3) the reduced χ^2. If $\chi^2 > 1$, we scale the uncertainty of the ratio by χ^2. The final ratio R is obtained as a weighted mean of the frequency ratios from all groups and measurement traps. Its statistical uncertainty ΔR is the larger of the internal and external errors[42]; see right side of Fig. 1. A variation of the polynomial order (second, third and fourth) results in an increase of the statistical uncertainty of the final ratio by ~10%.

The data were blindly analysed independently by two people, each using separately developed software. Both analyses yield similar external errors of 8×10^{-12} and internal errors of 7×10^{-12}, resulting in a Birge ratio of 1.14. The two weighted means differ by 4×10^{-12}. Thus, the combined final ratio is

$$R - 1 = 1.161(10)_{\mathrm{stat}} \times 10^{-9}$$

(All reported uncertainties are 1σ.) The uniqueness of the considered $^{187}Re^{29+}$ ions in the two electron configuration states is that the fractional difference in their masses is only 10^{-9}. Uncertainties due to systematic effects such as image charge shift, relativistic shift and higher-order magnetic and electric field (see, for example, ref. [43]) variations can be neglected. For these uncertainties to be at the level of 10% of the statistical uncertainty (10^{-12}), the cyclotron frequencies would have to be shifted by at least 10 kHz, which is excluded considering the present known performance of PENTATRAP. Therefore, the systematic uncertainties in the final ratio are well below the statistical uncertainty and hence can be neglected.

The ground and metastable states in $^{187}Re^{29+}$ belong to the Kr $4d^{10}\,{}^1S_0$ and $4d^9\,4f\,{}^3H_5$ electron configurations, respectively. Because the metastable state can only decay to the ground state—by a highly forbidden electric triacontadipole (E5) transition—its estimated lifetime is ~130 d. (We note that whereas optical transitions with similarly high multipolarities may feature much longer lifetimes[6], the high transition energy, together with hyperfine quenching, yields a lifetime in this regime.) Owing to repeated and fast processes of electron impact excitation followed by radiative decay inside the electron beam ion trap, low-lying metastable states and the ground state are roughly equally populated. In this case, the metastable ion fraction detected in PENTATRAP is approximately 50%. For the determination of the energy of the metastable state, seven measurement campaigns with three ions each were performed over the course of 12 days, during which not a single decay was detected.

From the final ratio, the energy of the metastable state with respect to the ground state can be calculated using $\Delta E_{\mathrm{Re}} = m(^{187}Re^{29+})(R-1)c^2$ (c, speed of light in vacuum). The uncertainty of the ion mass enters the total uncertainty reduced by a factor of $(R-1)$, and must be known to only $\Delta m/m \approx 10^{-4}$ to become negligible. Because the mass of the 29 removed electrons and their binding energies are well below that limit, we can simply use the neutral mass of ^{187}Re for the calculation, which gives $\Delta E_{\mathrm{Re}} = 202.2(17)$ eV.

Calculations of the energy difference

The high charge state and the complexity of the open $4d$ and $4f$ subshells calls for state-of-the-art theoretical methods to match the experimental accuracy. We apply three different fully relativistic approaches, namely, the multiconfiguration Dirac–Hartree–Fock (MCDHF) method[44,45] in two different implementations and the configuration interaction method employing Kohn–Sham orbitals, as implemented by the many-body script language Quanty[46]. The calculations also help to identify the observed metastable state. The first such state could be the $4d^9 4f^3\,{}^3P_0$ level with an energy of ~195 eV (see Fig. 2). This level may decay only to the ground state by a highly forbidden two-photon transition. However, ^{187}Re has a nuclear spin of $I = 5/2$ and thus a magnetic moment that couples this $^3P_0$ level to the nearby $^3P_1$ level, which can decay to the ground state by an E1 transition. The $^3P_0$ state thus acquires part of the probability of this allowed transition, a phenomenon called hyperfine quenching[47–50]. Following ref. [47] and using the

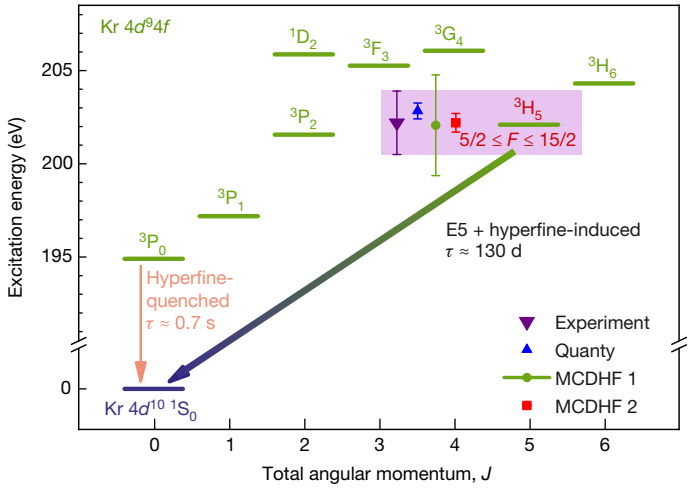

Fig. 2 | The $4d^{10}$ ground state and relevant $4d^9 4f$ excited electronic states of the $^{187}Re^{29+}$ ion. Experimental result (shaded area) and theoretical values obtained using MCDHF approaches in two different implementations (MCDHF 1 and 2) and a configuration-interaction calculation (Quanty). All error bars indicate 1σ uncertainty. The level structure is taken from the MCDHF 1 calculations. The lifetimes τ of the levels of interest are denoted and the main decay processes (hyperfine-induced/quenched and E5) are stated.

MCDFGME code[51], we estimate a lifetime of 0.7 s, which is too short to be observed. The observed state must then be the next metastable level, $4d^9 4f\,^3H_5$, which—neglecting quenching—can decay to the ground state only by an E5 transition with a lifetime of ~239 d. Decays to the levels just below—that is, to the $^3P_0$, $^3P_1$ and $^3P_2$ states—have very low probabilities because of their high multipolarities (M5, E4 and M3, respectively) and small photon energies. The $^3H_5$ state is also subject to hyperfine quenching; for example, its lifetime with a coupled atomic and nuclear angular momentum of $F = 7/2$ reduces to ~124 d. This corresponds to a width-to-transition energy ratio of 3×10^{-25}, enabling very-high-precision measurements. The states with $F = 9/2$ and $F = 11/2$ live 128 d, and other states coupled to more distant fine-structure levels have even longer lifetimes.

In the Quanty calculations of the transition energies, the relativistic Dirac Hamiltonian includes the Coulomb and Breit interactions between all electrons. The Fock space is spanned by multi-Slater-determinant states constructed from relativistic Kohn–Sham single-electron states, obtained from the density functional code FPLO[52], using the local spin density functional of ref. [53]. Within this calculation we explicitly include shells with principal quantum numbers $n < n_{max} = 7$. To extrapolate to $n_{max} = \infty$, we compare results for calculations with $n < 7$, $n < 6$ and $n < 5$. Allowing quantum fluctuations within the n=4 shells, that is, including configurations with holes in the 4*s*–4*d* shells and additional electrons in the 4*f* shell, we calculate the energies of the $4d^9 4f$ excited states in a first approximation. Allowing for a maximum of three electrons in the 4*f* shell suffices to calculate the excitation energy with the required accuracy. Next, we extend the configuration space to allow electrons to scatter between the n= 4, 5 and 6 shells, where at most three holes are excited. By successively adding further configurations, we can extrapolate the excitation energy of the $^3H_5$ metastable state to be between 202.41 eV and 203.26 eV.

In the MCDHF calculations, we optimize not only the mixing coefficients of the configurations but also the radial single-electron wave functions by self-consistently solving the corresponding radial Dirac equations. Quantum electrodynamics corrections to the excitation energy are estimated by the model potential method[54] and by computing the self-energy shift of the 4*d* and 4*f* valence electrons using effective potentials, which account for screening by the core electrons. One of the MCDHF calculations (MCDHF1) employs MCDFGME code[51], including full relaxation of all spectroscopic orbitals, as well as single and double excitations from all n=4 orbitals to the free single-electron states up to 5*d*, with a result of 202.1(27) eV. In the other computation (MCDHF2), using GRASP2018[55], we generate the set of configurations with single and double excitations from the n=4 states up to 9*h*, with the virtual orbitals optimized layer by layer. Subsequently, the effect of triple electron exchanges is accounted for in a configuration interaction approach. The convergence of the results is monitored while systematically expanding the configuration set, allowing us to estimate the uncertainty of the calculations and providing an extrapolated value of 202.2(5) eV.

Conclusion

Figure 2 shows a comparison of the three theoretical values with the experimental one. As a crosscheck, we also performed frequency ratio measurements (with less statistics) of the same metastable state in Os^{30+}, which is isoelectronic to Re^{29+}. We obtained $\Delta E_{Os} = 207(3)$ eV. As the electronic binding energy roughly scales with Z^2 (Z, atomic number), this higher energy is explained by the additional proton in Os ($Z = 76$) and the experimental result is again in agreement with the theoretical predictions, which are not explicitly given.

In summary, we have demonstrated a method of determining the excitation energies of extremely long-lived metastable states in HCIs that yields realistic measurement times if the metastable fraction in the atomic or ionic sample is at least 10% and the lifetime is longer than a few hours. In principle, with the precision achieved here for Re ions, it would also be possible to detect nuclear transitions with energies as low as 5 eV if the abundance of the isomeric nuclear state in the ions is comparable to that of the ground state.

Online content

Any methods, additional references, Nature Research reporting summaries, source data, extended data, supplementary information, acknowledgements, peer review information; details of author contributions and competing interests; and statements of data and code availability are available at https://doi.org/10.1038/s41586-020-2221-0.

1. Ludlow, A. D. et al. Optical atomic clocks. *Rev. Mod. Phys.* **87**, 637–701 (2015).
2. Katori, H. Optical lattice clocks and quantum metrology. *Nat. Photon.* **5**, 203–210 (2011).
3. Marti, G. E. et al. Imaging optical frequencies with 100 μHz precision and 1.1 μm resolution. *Phys. Rev. Lett.* **120**, 103201 (2018).
4. Brewer, S. M. et al. An $^{27}Al^+$ quantum-logic clock with systematic uncertainty below 10^{-18}. *Phys. Rev. Lett.* **123**, 033201 (2019).
5. Nicholson, T. et al. Systematic evaluation of an atomic clock at 2×10^{-18} total uncertainty. *Nat. Commun.* **6**, 6896 (2015).
6. Kozlov, M. G., Safronova, M. S., Crespo López-Urrutia, J. R. & Schmidt, P. O. Highly charged ions: optical clocks and applications in fundamental physics. *Rev. Mod. Phys.* **90**, 045005 (2018).
7. Seiferle, B. et al. Energy of the ^{229}Th nuclear clock transition. *Nature* **573**, 243–246 (2019).
8. Nauta, J. et al. Towards precision measurements on highly charged ions using a high harmonic generation frequency comb. *Nucl. Instrum. Methods Phys. Res. B* **408**, 285–288 (2017).
9. Cingöz, A. et al. Direct frequency comb spectroscopy in the extreme ultraviolet. *Nature* **482**, 68–71 (2012).
10. Shi, W., Redshaw, M. & Myers, E. G. Atomic masses of $^{32,33}S$, $^{84,86}Kr$, and $^{129,132}Xe$ with uncertainties ≤1 ppb. *Phys. Rev. A* **72**, 022510 (2005).
11. Eliseev, S. et al. Direct measurement of the mass difference of ^{163}Ho and ^{163}Dy solves the *Q*-value puzzle for the neutrino mass determination. *Phys. Rev. Lett.* **115**, 062501 (2015).
12. Crespo López-Urrutia, J. R. Frequency metrology using highly charged ions. *J. Phys. Conf. Ser.* **723**, 012052 (2016).
13. Ushijima, I. et al. Cryogenic optical lattice clocks. *Nat. Photon.* **9**, 185–189 (2015).
14. Huntemann, N. et al. Single-ion atomic clock with 3×10^{-18} systematic uncertainty. *Phys. Rev. Lett.* **116**, 063001 (2016).
15. Sanner, C. et al. Optical clock comparison for Lorentz symmetry testing. *Nature* **567**, 204–208 (2019).
16. Mehlstäubler, T. E. et al. Atomic clocks for geodesy. *Rep. Prog. Phys.* **81**, 064401 (2018).
17. Safronova, M. et al. Search for new physics with atoms and molecules. *Rev. Mod. Phys.* **90**, 025008 (2018).
18. Derevianko, A. & Pospelov, M. Hunting for topological dark matter with atomic clocks. *Nat. Phys.* **10**, 933–936 (2014).
19. McGrew, W. F. et al. Atomic clock performance enabling geodesy below the centimetre level. *Nature* **564**, 87–90 (2018).

20. Ong, A., Berengut, J. C. & Flambaum, V. V. in *Fundamental Physics in Particle Traps* 293 (Springer, 2014).
21. Dzuba, V. A. & Flambaum, V. V. Highly charged ions for atomic clocks and search for variation of the fine structure constant. *Hyperfine Interact.* **236**, 79–86 (2015).
22. Gillaspy, J. D. Highly charged ions. *J. Phys. B* **34**, R39 (2001).
23. Klaft, I. et al. Precision laser spectroscopy of the ground state hyperfine splitting of hydrogenlike $^{209}Bi^{82+}$. *Phys. Rev. Lett.* **73**, 2425–2427 (1994).
24. Morgan, C. A. et al. Observation of visible and UV magnetic dipole transitions in highly charged xenon and barium. *Phys. Rev. Lett.* **74**, 1716–1719 (1995).
25. Crespo López-Urrutia, J. R., Beiersdorfer, P., Savin, D. & Widmann, K. Direct observation of the spontaneous emission of the hyperfine transition $F = 4$ to $F = 3$ in ground state hydrogenlike $^{165}Ho^{66+}$ in an electron beam ion trap. *Phys. Rev. Lett.* **77**, 826–829 (1996).
26. Schiller, S. Hydrogenlike highly charged ions for tests of the time independence of fundamental constants. *Phys. Rev. Lett.* **98**, 180801 (2007).
27. Crespo López-Urrutia, J. R. The visible spectrum of highly charged ions: a window to fundamental physics. *Can. J. Phys.* **86**, 111–123 (2008).
28. Berengut, J. C., Dzuba, V. A., Flambaum, V. V. & Ong, A. Highly charged ions with E1, M1, and E2 transitions within laser range. *Phys. Rev. A* **86**, 022517 (2012).
29. Schippers, S. et al. Storage-ring measurement of the hyperfine induced $^{47}Ti^{18+}(2s2p\ ^3P_0 \rightarrow 2s^2\ ^1S_0)$ transition rate. *Phys. Rev. Lett.* **98**, 033001 (2007).
30. Träbert, E. et al. Time-resolved soft-X-ray spectroscopy of a magnetic octupole transition in nickel-like xenon, cesium, and barium ions. *Phys. Rev. A* **73**, 022508 (2006).
31. Träbert, E., Beiersdorfer, P. & Brown, G. V. Observation of hyperfine mixing in measurements of a magnetic octupole decay in isotopically pure nickel-like ^{129}Xe and ^{132}Xe ions. *Phys. Rev. Lett.* **98**, 263001 (2007).
32. Ritz, W. On a new law of series spectra. *Astrophys. J.* **28**, 237–243 (1908).
33. Gu, M. F. The flexible atomic code. *Can. J. Phys.* **86**, 675–689 (2008).
34. Brown, L. S. & Gabrielse, G. Geonium theory: physics of a single electron or ion in a Penning trap. *Rev. Mod. Phys.* **58**, 233–311 (1986).
35. Zschornak, G. et al. *Dresden Electron Beam Ion Sources: Latest Developments*. Technical Report (Technische Universität Dresden & DREEBIT GmbH, 2009); https://www.researchgate.net/publication/228896380_DRESDEN_ELECTRON_BEAM_ION_SOURCES_LATEST_DEVELOPMENTS.
36. Koivisto, H., Arje, J. & Nurmia, M. Metal ions from the volatile compounds method for the production of metal ion beams. *Rev. Sci. Instrum.* **69**, 785–787 (1998).
37. Roux, C. et al. The trap design of PENTATRAP. *Appl. Phys. B* **107**, 997–1005 (2012).
38. Repp, J. et al. PENTATRAP: a novel cryogenic multi-Penning-trap experiment for high-precision mass measurements on highly charged ions. *Appl. Phys. B* **107**, 983–996 (2012).
39. Cornell, E. A. et al. Single-ion cyclotron resonance measurement of $M(CO^+)/M(N_2^+)$. *Phys. Rev. Lett.* **63**, 1674–1677 (1989).
40. Feng, X. et al. Tank circuit model applied to particles in a Penning trap. *J. Appl. Phys.* **79**, 8–13 (1996).
41. Karthein, J. et al. QEC-value determination for $^{21}Na \rightarrow ^{21}Ne$ and $^{23}Mg \rightarrow ^{23}Na$ mirror-nuclei decays using high-precision mass spectrometry with ISOLTRAP at the CERN ISOLDE facility. *Phys. Rev. C* **100**, 015502 (2019).
42. Birge, R. T. The calculation of errors by the method of least squares. *Phys. Rev.* **40**, 207–227 (1932).
43. Smorra, C. et al. A parts-per-billion measurement of the antiproton magnetic moment. *Nature* **550**, 371–374 (2017).
44. Grant, I. P. Relativistic calculation of atomic structures. *Adv. Phys.* **19**, 747–811 (1970).
45. Desclaux, J. P., Mayers, D. F. & O'Brien, F. Relativistic atomic wave functions. *J. Phys. B* **4**, 631–642 (1971).
46. Haverkort, M. W. Quanty for core level spectroscopy – excitons, resonances and band excitations in time and frequency domain. *J. Phys. Conf. Ser.* **712**, 012001 (2016).
47. Indelicato, P., Parente, F. & Marrus, R. Effect of hyperfine structure on the 2^3P_1 and the 2^3P_0 lifetime in heliumlike ions. *Phys. Rev. A* **40**, 3505–3514 (1989).
48. Gould, H., Marrus, R. & Mohr, P. Radiative decay of the 2^3S_1 and 2^3P_2 states of heliumlike vanadium ($Z = 23$) and iron ($Z = 26$). *Phys. Rev. Lett.* **33**, 676–680 (1974).
49. Indelicato, P. et al. Hyperfine quenching and precision measurement of the $2^3P_0 - 2^3P_1$ fine structure splitting in heliumlike gadolinium (Gd^{62+}). *Phys. Rev. Lett.* **68**, 1307–1310 (1992).
50. Birkett, B. et al. Hyperfine quenching and measurement of the $2^3P_0 - 2^3P_1$ fine-structure splitting in heliumlike silver (Ag^{45+}). *Phys. Rev. A* **47**, R2454–R2457 (1993).
51. Indelicato, P. & Desclaux, J. MCDFGME: a multiconfiguration Dirac–Fock and general matrix elements program (2005).
52. Koepernik, K. & Eschrig, H. Full-potential nonorthogonal local-orbital minimum-basis band-structure scheme. *Phys. Rev. B* **59**, 1743–1757 (1999).
53. Perdew, J. P. & Wang, Y. Accurate and simple analytic representation of the electron-gas correlation energy. *Phys. Rev. B* **45**, 13244–13249 (1992).
54. Shabaev, V. M., Tupitsyn, I. I. & Yerokhin, V. A. QED-MOD: Fortran program for calculating the model Lamb-shift operator. *Comput. Phys. Commun.* **189**, 175–181 (2015).
55. Froese Fischer, C., Gaigalas, G., Jönsson, P. & Bierón, J. GRASP2018 – a Fortran 95 version of the General Relativistic Atomic Structure Package. *Comput. Phys. Commun.* **237**, 184–187 (2019).

Data availability

The datasets analysed in this study are available from the corresponding author.

Code availability

The experimental data were analysed using OriginLab and a self-written analysis script, which is available from the corresponding author. The Quanty code and its documentation are available from http://www.quanty.org. MCDHF 1 is described in ref. [51] and MCDHF 2 in ref. [55].

Acknowledgements This article comprises parts of the PhD thesis work of H.C., to be submitted to Heidelberg University, Germany. This work is supported by the German Research Foundation (DFG) Collaborative Research Centre SFB 1225 (ISOQUANT) and by the DFG Research UNIT FOR 2202. P.I. acknowledges partial support from NIST. Laboratoire Kastler Brossel (LKB) is supported by Unité Mixte de Recherche de Sorbonne Université, de ENS-PSL Research University, du Collége de France et du CNRS No. 8552. P.I., Y.N.N. and K.B. are members of the Allianz Program of the Helmholtz Association, contract number EMMI HA-216 'Extremes of Density and Temperature: Cosmic Matter in the Laboratory'. P.I. thanks J.-P. Desclaux for help in improving the MCDFGME code. This project received funding from the European Research Council (ERC) under the European Union's Horizon 2020 research and innovation programme under grant agreement number 832848 - FunI. Furthermore, we acknowledge funding and support by the International Max Planck Research School for Precision Tests of Fundamental Symmetries (IMPRS-PTFS) and by the Max Planck, RIKEN, PTB Center for Time, Constants and Fundamental Symmetries.

Author contributions The experiment was performed by R.X.S., M.D., A.R. and S.E. The data were analysed by R.X.S. and S.E. Theoretical calculations were performed by H.B., M.B., H.C., Z.H., M.W.H. and P.I. The manuscript was written by R.X.S., M.B., Z.H., M.W.H., P.I., J.R.C.L.-U. and S.E. and edited by S.U. and K.B. All authors discussed and approved the data as well as the manuscript.

Competing interests The authors declare no competing interests.

Additional information
Correspondence and requests for materials should be addressed to R.X.S. or S.E.
Peer review information *Nature* thanks Jens Dilling, Marianna Safronova and the other, anonymous, reviewer(s) for their contribution to the peer review of this work.
Reprints and permissions information is available at http://www.nature.com/reprints.